The Impact of Nitric Oxide Toxicity on the Evolution of the Glutathione Transferase Superfamily
A PROPOSAL FOR AN EVOLUTIONARY DRIVING FORCE*[S]

Alessio Bocedi[a1], Raffaele Fabrini[a1], Andrea Farrotti[a1], Lorenzo Stella[a], Albert J. Ketterman[b], Jens Z. Pedersen[c], Nerino Allocati[d], Peter C. K. Lau[e], Stephan Grosse[e], Lindsay D. Eltis[f], Antonio Ruzzini[f], Thomas E. Edwards[g], Laura Morici[a], Erica Del Grosso[a], Leonardo Guidoni[h,i], Daniele Bovi[h], Mario Lo Bello[c], Giorgio Federici[j], Michael W. Parker[k,l2], Philip G. Board[m], and Giorgio Ricci[a3]

From the Departments of [a]Chemical Sciences and Technologies and [c]Biology, University of Rome, Tor Vergata, Via della Ricerca Scientifica 1, 00133 Rome, Italy, the [b]Institute of Molecular Biosciences, Mahidol University, Salaya Campus, Nakhon Pathom 73170, Thailand, the [d]Department of Biomedical Sciences, University of Chieti "G. D'Annunzio," Via dei Vestini 31, 66013 Chieti, Italy, the [e]National Research Council Canada, 6100 Royalmount Avenue, and Departments of Chemistry and Microbiology & Immunology, McGill University, 3775 Montreal, Quebec, Canada, the [f]Department of Microbiology and Biochemistry, Life Sciences Institute, University of British Columbia, 2350 Health Sciences Mall, Vancouver, British Columbia, Canada, the [g]Seattle Structural Genomics Center for Infectious Disease, USA, and Emerald BioStructures Inc., Bainbridge Island, Washington 98110, the [h]Department of Physics, University of Rome "Sapienza," Rome 00185, Italy, the [i]Department of Physical and Chemical Sciences, University of L'Aquila, 67100 L'Aquila, Italy, the [j]Children's Hospital IRCCS "Bambin Gesù," 00165 Rome, Italy, the [k]ACRF Rational Drug Discovery Centre and Biota Structural Biology Laboratory, St. Vincent's Institute of Medical Research, 9 Princes Street, Fitzroy, 3065 Victoria, Australia, the [l]Department of Biochemistry and Molecular Biology, Bio21 Molecular Science and Biotechnology Institute, University of Melbourne, Parkville, 3010 Victoria, Australia, and the [m]Molecular Genetics Group, John Curtin School of Medical Research, Australian National University, Canberra, 2601 Australian Capital Territory, Australia

Background: Why do ancestral GSTs utilize cysteine/serine as catalytic residues, whereas more recently evolved GSTs utilize tyrosine?
Results: Only the more recently evolved GSTs display enough affinity to bind and make harmless the toxic DNDGIC (a natural NO carrier).
Conclusion: GST evolution could be linked to the defense against NO.
Significance: This represents a further piece in the puzzle of evolutive adaptation to NO toxicity.

Glutathione transferases (GSTs) are protection enzymes capable of conjugating glutathione (GSH) to toxic compounds. During evolution an important catalytic cysteine residue involved in GSH activation was replaced by serine or, more recently, by tyrosine. The utility of these replacements represents an enigma because they yield no improvements in the affinity toward GSH or in its reactivity. Here we show that these changes better protect the cell from nitric oxide (NO) insults. In fact the dinitrosyl·diglutathionyl·iron complex (DNDGIC), which is formed spontaneously when NO enters the cell, is highly toxic when free in solution but completely harmless when bound to GSTs. By examining 42 different GSTs we discovered that only the more recently evolved Tyr-based GSTs display enough affinity for DNDGIC ($K_D < 10^{-9}$ M) to sequester the complex efficiently. Ser-based GSTs and Cys-based GSTs show affinities 10^2–10^4 times lower, not sufficient for this purpose. The NO sensitivity of bacteria that express only Cys-based GSTs could be related to the low or null affinity of their GSTs for DNDGIC. GSTs with the highest affinity (Tyr-based GSTs) are also over-represented in the perinuclear region of mammalian cells, possibly for nucleus protection. On the basis of these results we propose that GST evolution in higher organisms could be linked to the defense against NO.

Glutathione transferases (GSTs) are a superfamily of enzymes expressed in almost all living organisms, from bacteria to humans, and are devoted to cell protection, acting both as catalysts and as ligandins (1, 2). Microsomal GSTs, mitochondrial GSTs, and cytosolic GSTs are the three families that represent almost all GSTs in living systems. Based on sequence similarity, substrate and inhibitor sensitivity, and immunological properties, cytosolic GSTs have been grouped into more than 16 gene-independent GST classes identified by Greek letters (3, 4). A common ability of all GSTs is to bind reduced glutathione (GSH) and lower the pK_a of its sulfhydryl group thereby increasing its reactivity toward dangerous alkylating toxins, hydroxy-nonenals, peroxides, and disulfides (1, 5). GSH activation is favored by a crucial residue at the active site (Tyr, Ser, or Cys) whose hydroxyl or sulfhydryl

group is within hydrogen bonding distance of the sulfur atom of GSH.

From an evolutionary point of view, it is well accepted that GSTs evolved from an ancestral thioredoxin-like protein similar to the proteins forming the thiol reductase superfamily (1, 6). Indeed, the most ancient GSTs possess an important cysteine in the active site involved in the GSH activation. This residue is present in the Beta class bacterial GSTs, in the Omega class (also present in mammals), and in other distinct GSTs expressed in many parasites and microorganisms. In a parallel or successive evolutionary step, a serine residue replaced Cys in this activation role. This residue is found in the Theta, Tau, Delta, Zeta, Epsilon, and Phi classes GSTs. Finally, the most recently evolved GSTs possess a tyrosine residue involved in GSH activation (*e.g.* Alpha, Pi, Mu, Sigma, *Plasmodium falciparum* GST, *Onchocerca volvulus* GST, and Schistosoma GSTs). No convincing explanations have been proposed for the evolutionary necessity or utility of these replacements.

As will be shown here, these three distinct subfamilies (Cys-based GSTs, Ser-based GSTs, and Tyr-based GSTs) are able to bind GSH with similar affinities and also to cause a very efficient activation of its sulfhydryl group. Even the different co-substrate specificity or ability to catalyze peculiar reactions found in specific isoenzymes does not represent a reasonable cause for the Cys/Ser/Tyr replacements because many GSTs display similar or different co-substrate specificity or peculiar catalysis irrespective of the presence of Tyr, Ser, or Cys in the active site. Here we show for the first time that these replacements may be selected to better protect the organism from nitric oxide (NO) insult.

NO is a multifunctional molecule that is used with different degrees of complexity in all organisms. The high affinity of NO for transition metal centers like heme, and the rapid reaction of NO with thiols (to form *S*-nitrosothiols) and oxygen-derived free radicals can explain many of its biological and pathological properties (7). However, when NO enters the cell or is produced inside the cell, a further spontaneous reaction occurs, involving endogenous thiols and labile iron, leading to the formation of dinitrosyl·iron complexes. These compounds display paramagnetic properties ($g = 2.03$) and can function as NO carriers by virtue of their relatively high stability (minutes) compared with free NO (seconds) (8). The low mass dinitrosyl·diglutathionyl iron complex (DNDGIC)[4] (Fig. 1*A*) is probably the most abundant dinitrosyl·iron complex formed inside the cell in case of NO insult, because GSH is always present in the cytosol at high concentrations (1–10 mM). However, DNDGIC is also dangerous to the cell because, even at micromolar levels, it inactivates irreversibly glutathione reductase, a key enzyme fundamental for cellular redox balance (9, 10).

Thus it is not surprising that this iron complex has never been found *in vivo* in the free state but always in a harmless form bound to "unknown" proteins (8). In hepatocytes and in other mammalian cells these proteins have recently been identified as GSTs (11–13). Mammalian GSTs, in particular the

Alpha, Pi, and Mu class GSTs, can accomplish this function by virtue of their high expression in all tissues (*e.g.* 0.5–0.8 mM in liver) and their strong affinity for this complex ($K_D = 10^{-9}$–10^{-10} M) (12, 14). It was also noted that one Ser-GST (GSTT2-2) and one Cys-GST (GSTB1-1) display less affinity suggesting the possibility of an evolutionary development of this interaction (12).

In the present work we have studied the interaction of GSTs with DNDGIC by means of EPR, kinetics, and site-directed mutagenesis experiments on many purified GST isoenzymes, whose structures (in complex with GSH) have been solved previously, in combination with *ab initio* calculations and docking studies. Our data demonstrate that only the more recently evolved GSTs, *i.e.* the Tyr-based GSTs, are able to protect the cell efficiently from the cytotoxic activity of DNDGIC. The structural and electrostatic properties of Cys-based GSTs and Ser-based GSTs provide the explanation for their lower affinity for DNDGIC. Interestingly, the GSTs with the greatest affinity are also localized in the perinuclear region suggesting that, beside key cytosolic enzymes, further targets of protection may be DNA or the transcription machinery localized inside the nucleus.

EXPERIMENTAL PROCEDURES

Protein Expression and Purification—GSTs were expressed and purified as reported previously. In particular, Tyr-GST: *h*GSTA1-1 (12), *h*GSTM2-2 (12), *h*GSTP1-1 (12), *h*GSTA2-2 (15), and *h*GSTA3-3 (16), *O. volvulus* GST2 (17), *Schistosoma hematobium* GST (18), *P. falciparum* GST (19), and squid GST (20); Ser-GSTs: *h*GSTT2-2 (21), Phi 1 GST Mais (22), *h*GSTZ (23), *Anopheles dirus* GSTD3-3 (24), *A. dirus* GSTD4-4 (25), *A. dirus* GSTD5-5 (26); Cys-GSTs: *h*GSTO1-1 (27) *Proteus mirabilis* GSTB1-1 (12), *Sphingomonas paucimobilis* GST (supplemental Methods), *Burkholderia xenovorans* GST (28), *Ochrobactrum anthropi* GST (29), and *Coccidioides immitis* GST (30). Mutant GSTs were expressed and purified as follows: Y7F *h*GSTP1-1 (31), Y7C *h*GSTP1-1 (31), S11A *h*GSTT2-2 (32), C10A GST from *P. mirabilis* (33), and C10A GST from *O. anthropi* (34).

DNDGIC Synthesis—DNDGIC was prepared essentially as described previously (14). Briefly, 1 ml of 0.5 mM FeSO$_4$ (dissolved in degassed water to avoid rapid oxidation to the ferric state) was added to 10 ml (final volume) of 0.1 mM potassium phosphate buffer, pH 7.4, containing 20 mM GSH and 2 mM GSNO (25 °C). After 10 min, the reaction was almost complete, and the resulting stock solution of DNDGIC (50 µM) was stable for at least 3 h.

DNDGIC Binding—The interaction of DNDGIC with Tyr-GSTs and Ser-GSTs has been studied by means of inhibition experiments using the classical enzymatic reaction, *i.e.* GSH (1 mM), 1-chloro-2,4-dinitrobenzene (1 mM) in 0.1 M potassium phosphate buffer. The procedure was identical to that described previously (12). Inhibition kinetic data were fitted to the classical equation of competitive inhibition by assuming that the binding of DNGIC competes with the binding of free GSH in the G-site. As demonstrated previously, this approach provides K_D values very similar to those obtained using stopped-flow or fluorescence quenching methods (12). As

---

[4] The abbreviations used are: DNGIC, dinitrosyl·glutathionyl·iron complex; DFT, density functional theory; DNDGIC, dinitrosyl·diglutathionyl·iron complex; EPR, electron paramagnetic resonance; PDB, Protein Data Bank.

many GSTs show negative cooperativity in DNDGIC binding, for the sake of simplicity we only reported K_D values for the high affinity binding site.

EPR Experiments—Due to the very low affinity of many Cys-GSTs for DNDGIC, EPR binding experiments was the preferred approach to determine K_D values, because it is performed with enzyme and complex concentrations 10–100 times higher than those used for kinetic studies. Still, for some GSTs a detectable amount of bound DNGIC could not been obtained. In these cases we assumed that the bound species was less than 5% and this percent has been used to calculate a limit value for K_D as reported in Table 1. This limit value is not identical for all low affinity GSTs as it also depends on the enzyme concentrations used in the EPR experiments. In a typical EPR experiment, GST samples were prepared in 0.1 M potassium phosphate buffer, pH 7.4, with DNDGIC added from a freshly made stock solution. EPR measurements were made at room temperature (22–25 °C) with a Bruker ESP300 X-band instrument (Bruker, Karlsruhe, Germany) equipped with a high sensitivity TM_{110}-mode cavity. To optimize instrument sensitivity, spectra were recorded using samples of 80 μl contained in flat glass capillaries (inner cross-section 5 × 0.3 mm). Unless otherwise stated, spectra were measured over a 200 G range using 20 milliwatt power, 2.0 G modulation, and a scan time of 42 s; typically 4–40 single scans were accumulated to improve the signal to noise ratio. High resolution spectra were recorded with 0.1 G modulation and 2 milliwatt power.

Geometry of the DNGIC·GST Complexes—DNGIC·GST complex geometry and partial charges were obtained by performing density functional theory (DFT) calculations in the Kohn-Sham ansatz (35, 36). Because these calculations are computationally demanding, our calculations were limited to a partial GST·DNGIC complex, including the iron atom, NO groups, and the side chains of the GSH cysteine and GST catalytic residue. Minimum energy geometry and charges for each DNGIC·GST complex (*i.e.* with Tyr, Ser, or Cys as the catalytic residue) were evaluated with the "Broken Symmetry" approach (37), using ORCA software (38, 39), and following the method previously used for a similar system (40). The comparison between the only available crystallographic structure of a DNGIC·GST complex (human GSTP1-1, PDB code 1ZGN) and the results of the DFT calculations reveals a similar geometry (Fig. 1 and Table 1), except for the position of NO groups, which are coordinated to protein residues in GSTP1-1 (which are obviously absent in the DFT calculations) (31).

Docking Calculations—Docking calculations were performed using AutoDock4, and its graphical user interface AutoDockTools (41). To mimic the real system, in which a coordination bond exists between the catalytic residue and the DNGIC, docking simulations were performed according to the recently developed method called "covalent" docking (42). In this technique a bond is formed between the ligand and the side chain of the proper receptor binding site residue (the catalytic residue in the case of GSTs). The ligand-side chain structure is then treated as flexible, allowing the rotation around some dihedrals. In our system we selected those involving the iron atom, GSH cysteine, and GST catalytic residue side chain. To determine the DNGIC/protein interaction free energy differ-

ence, the free energy of the ligand in solution and the interaction between the free catalytic side chain and the rest of GST in the unbound protein must be subtracted from the ligand-side chain/protein interaction free energy. Bond geometry and atom charges obtained in the DFT calculations were used for the ligand·side chain complex (iron atom, NO groups, Cys side chain of GSH, and catalytic residue of GST). With regard to the remaining atoms of the complex, in the single available structure of a DNGIC·GST complex (human GST P1-1, PDB code 1ZGN) the GSH of DNGIC is located in the same position of the GST·GSH complex (PBD code 6GSS), with a root mean square deviation of ~0.8 Å. For this reason, in the docking simulations GSH (with the exclusion of the Cys side chain) was left in the same conformation of the corresponding GST·GSH complex crystallographic structure, and Gasteiger charges were used for these atoms (43). Control simulations on selected GSTs showed that releasing the GSH rotational degrees of freedom did not significantly improve the docking free energy. With the exception of the catalytic residue, no flexibility was taken into account for protein atoms, for which Kollman charges were used (44). The cubic grid used in potential calculations was formed by 70 × 70 × 70 points (0.375 Å spacing), and was centered on the hydroxyl oxygen or sulfur atom of the GST catalytic residue. The docking was performed with the Lamarckian Genetic Algorithm, and default parameters.

Docking simulations, as described above, included an energy of interaction between GST and DNGIC, which lacks contribution of the Tyr, Ser, or Cys coordination bond. Based on site-directed mutagenesis of GSTP1-1, it was assumed that the coordination due to its Tyr residue (pK_a = 9.8) gives a contribution of −4.1 kcal/mol. This energy value has been properly modified as a function of the different pK_a of Tyr in each Tyr-GST (Table 2) according to the following expression.

$$E = -4.1 - (RT\ln 10)(9.8 - pK_a) \quad \text{(Eq. 1)}$$

The mutant of the essential cysteine in *O. anthropi* GST (pK_a = 7.6) is about 270 times lower affinity than the wild-type (see Table 2), which correspond to an energy contribution due to this residue of −3.3 kcal/mol. As above, this value must be corrected considering the specific pK_a of each Cys-GSTs, according to Equation 2.

$$E = -3.3 - (RT\ln 10)(7.6 - pK_a) \quad \text{(Eq. 2)}$$

As suggested by a specific mutant of the essential Ser in the human GSTT2-2, no energy contribution has been considered due to this residue because of very high pK_a of Ser in all Ser-GSTs.

pK_a values of Tyr, Ser, and Cys catalytic residues within the active site of each available GST structure were evaluated using Poisson-Boltzmann electrostatic calculations performed with APBS software (45), assuming pK_a values of 10.1, 13.0, and 8.7, respectively, for the isolated Tyr, Ser, and Cys residues. APBS input files were generated on the PDB2PQR server (46) using PARSE continuum electrostatics force field (47).

Isoelectric points (pI) of GSTs were evaluated based on PDB codes as folded structural values obtained by PDB2PQR, using PARSE continuum electrostatics force field and the PROPKA
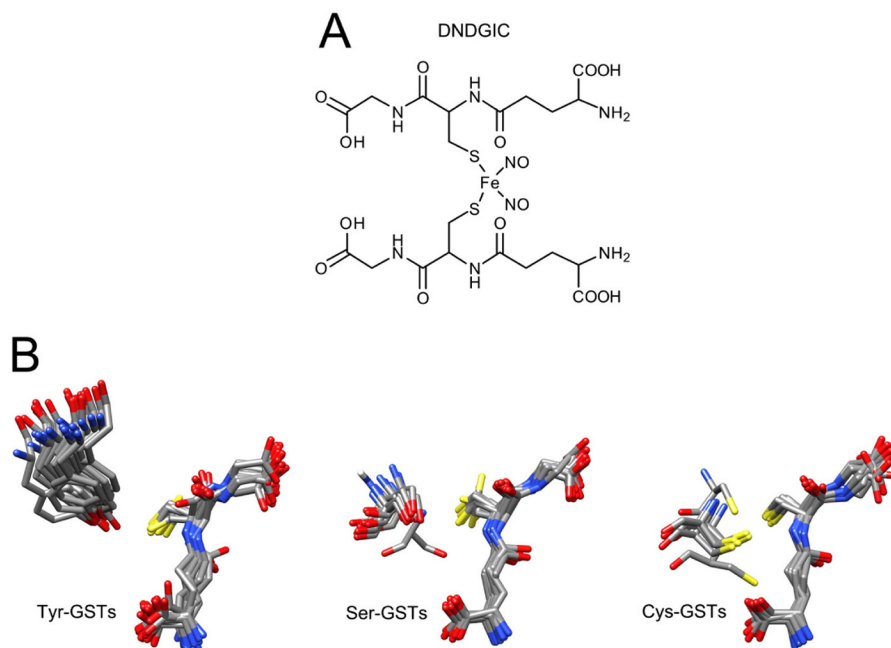
FIGURE 1. **Formula of DNDGIC and structures of GSH bound to GSTs.** *A,* chemical structure of DNDGIC. *B,* superimposition of GSH in the crystallographic structures of GSTs (for the 20 Tyr-GSTs, 14 Ser-GSTs, and 8 Cys-GSTs listed in Table 2). Catalytic residues are also shown. The only divergent crystal structures are *h*GSTZ1-1 (a Ser-GST) and *h*GSTO1-1 (a Cys-GST).

calculator (46). Molecular graphics pictures were created by UCSF Chimera (48).

RESULTS

Binding and Activation of GSH in the Three GST Subfamilies— GSTs are dimeric proteins that display a characteristic fold very similar in both the more ancient isoenzymes (Cys-GSTs and Ser-GSTs) as well as in the more recently evolved GSTs (Tyr-GSTs) (1). GSH binds to a specific protein region, termed the G-site, assuming an extended conformation that is very similar in all GST subfamilies (Fig. 1*B*). One of the most significant differences among the three subfamilies is that the essential Tyr residue involved in GSH activation is part of β-strand 1, whereas critical residues in Ser-GSTs and Cys-GSTs are located in the loop, which connects the first β-strand and the α-helix 1 (Fig. 2*A*). This difference, however, does not appear to have important effects on the affinity for GSH. In fact, K_m values for GSH were determined experimentally in the present study for 10 different GSTs and those obtained from the literature (21 GSTs), display values ranging from 0.5 to 5×10^{-4} M without any significant difference among subfamilies (average K_m values are $2.4 (\pm 0.6) \times 10^{-4}$ M, $4.1 (\pm 0.8) \times 10^{-4}$ M, and $3 (\pm 1) \times 10^{-4}$ M for Tyr-GSTs, Ser-GSTs, and Cys-GSTs, respectively) (Table 1). Considering that the GSH levels in most cells range from 1 to 10 mM (49), it is clear that all these GSTs work *in vivo* under nearly saturating conditions (Fig. 2*B*). Moreover, the facilitated deprotonation of GSH, a fundamental event to enhance its chemical reactivity, occurs efficiently in representative members of all these GST subfamilies. For example, in the Alpha, Pi, and Mu GSTs (all Tyr-GSTs) the pK_a of the bound GSH shifts from 9.0 to 6.0 – 6.8 (50, 51), but similar lowered values have been found for the *P. mirabilis* GSTB1-1 (Cys-GST) both in the reduced (pK_a = 5.2) and oxidized form (pK_a = 6.4) (33), and in the *Lucilia cuprina* GST and in the human GSTT2-2 (both Ser-GSTs) (pK_a = 6.6 and

6.2, respectively) (21, 51). In conclusion, the Cys/Ser/Tyr replacements during evolution have not been selected to reach a better affinity or activation of GSH.

DNDGIC Binding to GST Subfamilies— The paramagnetic DNDGIC probably has the highest affinity of any natural low-mass compound for the Tyr-GSTs (*e.g.* human GSTP1-1, GSTA1-1, and GSTM2-2) (12, 14). The dissociation constants found for these Tyr-GSTs range between 10^{-10} (GSTA1-1) and 10^{-9} M (GSTP1-1 and GSTM2-2), values near those found for hormone/receptor interactions and 100 lower than that displayed by the most potent GST inhibitors designed as drugs to lower the GST-mediated resistance against chemotherapeutics (52). The present study examines the DNDGIC binding to many GST isoenzymes including the Ser-GST and Cys-GST subfamilies. As shown in Table 1 and Fig. 2*C*, K_D values obtained in the present study for 16 different GSTs, using kinetics and/or EPR approaches, or coming from our previous study (11), depict a convincing scenario of differential affinity. Although almost all examined Tyr-GSTs show extraordinary affinity for DNDGIC (K_D ranging from 10^{-11} to 10^{-9} M), the Ser-GST subfamily displays 10^2–10^4 times lower affinity (K_D from 10^{-7} to 10^{-6} M). The Cys-GSTs show even higher dissociation constants ($K_D > 10^{-7}$ M). Thus, it is evident that the most competent GSTs for the binding of DNDGIC are the Tyr-GSTs, which are also the more recently diverged isoenzymes, suggesting that an evolutionary pressure has selected this residue for optimization of this interaction. An interesting exception among the Tyr-GSTs is represented by the *P. falciparum* GST. This particular transferase shows structural properties similar to the Mu class GSTs but 100 times less affinity for DNDGIC than all other Tyr-GSTs (Table 1). As discussed below, this exception may confirm the link between GST evolution and NO protection.
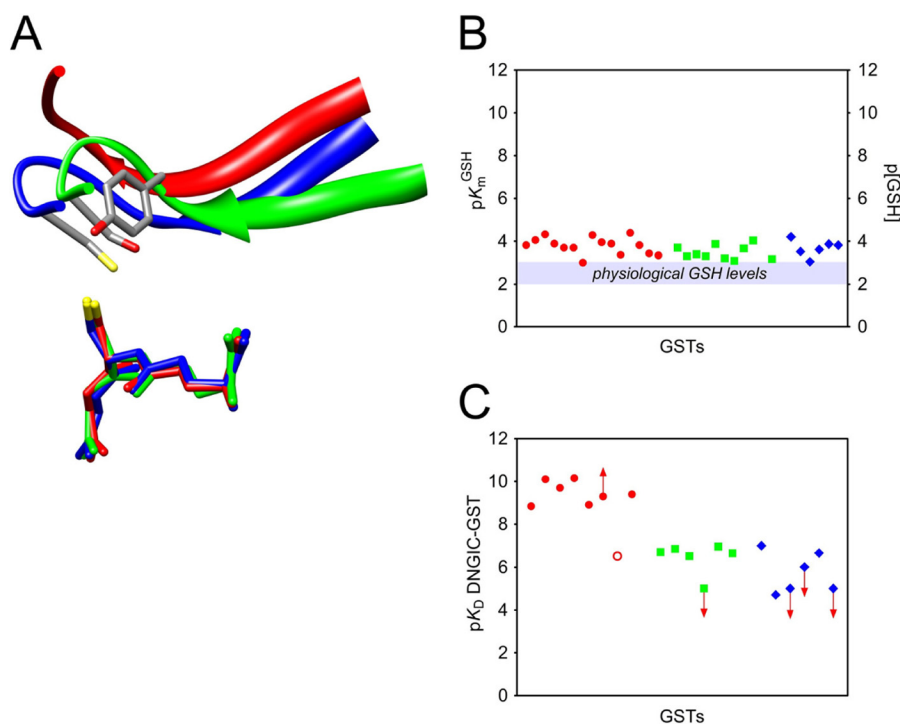
FIGURE 2. **Orientation of the catalytic residue and kinetic constants for the three GSTs subfamilies.** *A,* representative structures for Tyr-GSTs (PDB code 1K3L) (*red*), Ser-GSTs (PDB code 3LJR) (*green*), and Cys-GSTs (PDB code 1EEM) (*blue*). The segment of protein backbone containing the catalytic residue is shown in a *ribbon* representation, whereas GSH is reported as *sticks*. The Tyr residue is located on the β1 strand, whereas Ser and Cys residues are on the $\beta1\alpha1$ loop. *B,* experimental K_m values for GSH binding to Tyr-GSTs (*red circle*), Ser-GSTs (*green square*), and Cys-GSTs (*blue triangle*); starting from the left: data refer to GSTs in the same sequence as reported in Table 1 (excluding the five mutants). *C,* experimental K_D values for DNGIC/GST interaction. Tyr-GSTs (*red circle*), *Pf*GST (*red open circle*), Ser-GSTs (*green square*), Cys-GSTs (*blue triangle*). For a few GSTs lacking detectable amounts of bound DNGIC, only a limiting lower value of K_D is reported. *Red arrow* indicates that the true K_D could be even higher (*red arrow* ↓) or lower (*red arrow* ↑). Starting from left: data refer to GSTs in the same sequence as that reported in Table 1 (excluding the five mutants).

Useful information about the role of each catalytic residue in all three GST subfamilies came from isosteric point mutations (Table 1). The replacement of Tyr-7 by Phe in *h*GSTP1-1 and Cys-10 by Ala in *O. anthropi* GST lower strongly the affinity for DNDGIC (about 1000 and 300 times, respectively), suggesting a crucial role of −OH and −SH moieties of these residues in the DNDGIC binding. Additional thermodynamic computations about these mutants are reported below. Conversely, the isosteric point mutation of Ser-11 by Ala in *h*GSTT2-2 indicated a scarce contribution of this residue in the DNDGIC stabilization in the G-site.

Structure of the G-site and Acid-base Properties of the Tyr/Ser/Cys Residues Are the Causes of Different Affinities—Only one crystal structure of DNDGIC bound to a protein has been solved, *i.e.* that involving the human GSTP1-1 (a Tyr-GST) (31). The complex binds to the G-site so that the iron center is ligated to two NO ligands, to one GSH occupying the same position as found in structures of other GST·GSH complexes, and to the deprotonated hydroxyl group of Tyr-7 that completes the coordination shell. Thus, in this interaction DNDGIC looses one GSH molecule, which is replaced by the Tyr-7 residue (31). It is likely that all other Tyr-GSTs bind the complex in an identical way. Considering the similarity of the EPR spectra (Fig. 3), it is also plausible that a similar binding modality is also adopted by the other two GST subfamilies, where a Ser or Cys residue replace Tyr. To obtain structural models of the complex in the different GSTs and to estimate the binding affinity of DNDGIC to isoenzymes for which experi-

mental data could not be gathered, docking calculations were performed. For determining the complex bond length, angles, and partial charge distribution needed for these studies, we first performed *ab initio* calculations for the three different complexes involving the DNGIC moiety and the active site Ser, Cys, or Tyr residue as a fourth ligand (see "Experimental Procedures" and also supplemental Methods for a more detailed description). This theoretical approach was validated with GSTP1-1 in which the resultant model showed an almost perfect overlap with that observed in the crystal structure of DNGIC·GSTP1-1 complex (Fig. 4*A* and supplemental Table S1). The corresponding DNGIC structures with Ser and Cys are shown in Fig. 4*B* and their geometric, electrostatic and magnetic properties reported in supplemental Tables S1–S3.

These theoretical models have been employed for docking calculations using AutoDock software (41) in the "covalent docking" mode (42), *i.e.* by forming the coordination bond, and then exploring the different conformations resulting from rotation of dihedrals of the complex and the side chain (see "Experimental Procedures"). The resulting free energies of interaction (Fig. 4*C* and supplemental Table S4) indicate a significantly weaker interaction for Cys-GSTs as compared with the Tyr-GSTs, while Ser-GSTs exhibit an intermediate behavior. Obviously these data, which consider only electrostatic, van der Waals, and hydrophobic interactions, do not take into account the energy contribution due to the formation of the coordination bond between iron and the critical residue. However, an estimate of the free energy involved in this metal-ligand bond

TABLE 1

K_m **for GSH (determined experimentally in the present study or available from the literature) and K_D values for DNGIC·GST complex coming from kinetic or EPR experiments**

For many Cys-GSTs, the lack of detectable amounts of bound DNGIC in EPR experiments allows us to report only a lower limiting value for K_D.

PDB ID	GSTs	Experimental K_m for GSH[a,b]	Experimental K_D for DNGIC-GST binding[a]
		M	M
Tyrosine subfamily			
6GSS	*h*GSTP1-1	1.5×10^{-4}	1.5×10^{-9}
	*h*GSTP1-1 Y7C	7.3×10^{-4}	1.3×10^{-6}
	*h*GSTP1-1 Y7F	1.6×10^{-4}	1.5×10^{-6}
1GLP	*m*GSTYfYf	0.9×10^{-4}	
1TU8	*O. volvulus* GST2	0.5×10^{-4}	
1K3L	*h*GSTA1-1	1.3×10^{-4}	8.0×10^{-11}
2WJU	*h*GSTA2-2	2.0×10^{-4}	2.0×10^{-10}
1TDI	*h*GSTA3-3	2.0×10^{-4}	7.0×10^{-11}
1GUL	*h*GSTA4-4	1.0×10^{-3}	
1GSU	*c*GSTM1-1	0.5×10^{-4}	
2AB6	*h*GSTM2-2	1.1×10^{-4}	1.2×10^{-9}
6GST	*r*GSTM3-3	1.3×10^{-4}	
1M9A	*S. japonicum* GST	4.3×10^{-4}	
1OE7	*S. haematobium* GST	4.0×10^{-4}	$<5.0 \times 10^{-10}$
1Q4J	*P. falciparum* GST	1.5×10^{-4}	3.0×10^{-7}
1U3I	*S. mansoni* GST	3.7×10^{-4}	
1GSQ	Squid GSTS	4.5×10^{-4}	4.0×10^{-10}
Serine subfamily			
1AXD	Phi 1 GST Mais	2.0×10^{-4}	2.0×10^{-7}
	L. cuprina GST	5.0×10^{-4}	
1JLV	*Ad*GSTD3-3	4.0×10^{-4}	1.4×10^{-7}
3LJR	*h*GSTT2-2	5.0×10^{-4c}	3.0×10^{-7}
	*h*GSTT2-2 S11A	3.0×10^{-4}	4.0×10^{-7}
1FW1	*h*GSTZ1-1	1.3×10^{-4d}	$\gg 10^{-6}$
1GWC	*Ta*GSTU4-4	6.2×10^{-4}	
1PN9	*Ag*GSTB1-6	8.0×10^{-4}	
1R5A	*Ad*GSTD5-5	2.1×10^{-4}	1.1×10^{-7}
2C3Q	*h*GSTT1-1	1.0×10^{-4e}	
3F63	*Ad*GSTD4-4	6.7×10^{-4}	2.2×10^{-7}
Cysteine subfamily			
1EEM	*h*GSTO1-1	0.6×10^{-4f}	1.1×10^{-7}
2PMT	*P. mirabilis* GSTB1-1	3.0×10^{-4}	$>10^{-5}$
	P. mirabilis GSTB1–1 C10A	8.0×10^{-4}	$\gg 2 \times 10^{-5}$
1F2E	*S. paucimobilis* GST	9.0×10^{-4}	$\gg 10^{-6}$
2DSA	*B. xenovorans* GST	2.4×10^{-4}	$\gg 10^{-6}$
2NTO	*O. anthropi* GST	1.3×10^{-4}	2.2×10^{-7}
	O. anthropi GST C10A	140×10^{-4}	6.0×10^{-5}
3N5O	*C. immitis* GST	1.5×10^{-4}	$\gg 10^{-5}$

[a] Values determined in the present study are reported in bold, whereas values in normal characters are obtained from literature. References reported in the supplemental Methods.
[b] The co-substrate used for K_m determination is 1-chloro-2,4-dinitrobenzene.
[c] The co-substrate used for K_m determination is 1-menaphtyl sulfate.
[d] The co-substrate used for K_m determination is (±)-2–2bromo-3-(4-nitrophenyl) propanoic acid.
[e] The co-substrate used for K_m determination is iodohexane.
[f] The co-substrate used for K_m determination is S-(phenacyl)glutathione.

can be made from experimental data of certain GSTs belonging to the three subfamilies. It is known that replacement of Tyr-7 by Phe in *h*GSTP1-1 lowers the affinity of the enzyme for DNDGIC from a K_D of 10^{-9} to 10^{-6} M (31) (see Table 1). Thus the contribution to the stabilization of the complex in the G-site due to the coordination link of the iron with Tyr-7 can be estimated to be ~4.1 kcal/mol. Replacement of Cys-10 by Ala in *P. mirabilis* GSTB1-1 (Cys-GST) also lowers the affinity, although a precise estimation value of the energy contribution cannot be calculated due to the poor affinity of both native and mutated enzymes (Table 2). More reliable data have been obtained using the mutant of a second Cys-GST enzyme, *O. anthropi* GST. The affinity of C10A is about 270 times less than in the native enzyme, corresponding to a loss of 3.3 kcal/mol. On the contrary, the mutation of Ser-11 ($pK_a = 11.3$) by Ala in *h*GSTT2-2 (Ser-GST) does not modify significantly the affinity for the complex (Table 1), suggesting a null or very scarce involvement of this residue in the stabilization of the complex in the active site. To calculate this energy contribution for all

other GSTs present in this study, a further refinement must be made by considering the different pK_a of Tyr and Cys in each Tyr- and Cys-GSTs (see "Experimental Procedures"). The corrected theoretical values (Table 2) are in good agreement with the experimental values for 20 purified GSTs (Fig. 4*D*). Thus, we extended our theoretical analysis to other 22 GSTs, confirming that only the Tyr-GSTs have greatly optimized their binding to DNDGIC.

The relatively poor affinity found experimentally for the Ser-GSTs is straightforwardly explained on the basis of the very high pK_a of Ser ($pK_a = 13$) given that only the deprotonated hydroxyl group may bind the iron ion. A structure-based calculation of the pK_a of the Ser residue in all the Ser-GSTs (by executing Poisson-Boltzmann electrostatic calculations with the Adaptive Poisson-Boltzmann Solver (APBS) software (45)) indicated that the protein environment only slightly increases the acidity of this residue (the average pK_a for all tested Ser-GSTs is 12). Therefore, only traces of deprotonated Ser residues can be present at physiological pH values. Conversely, the
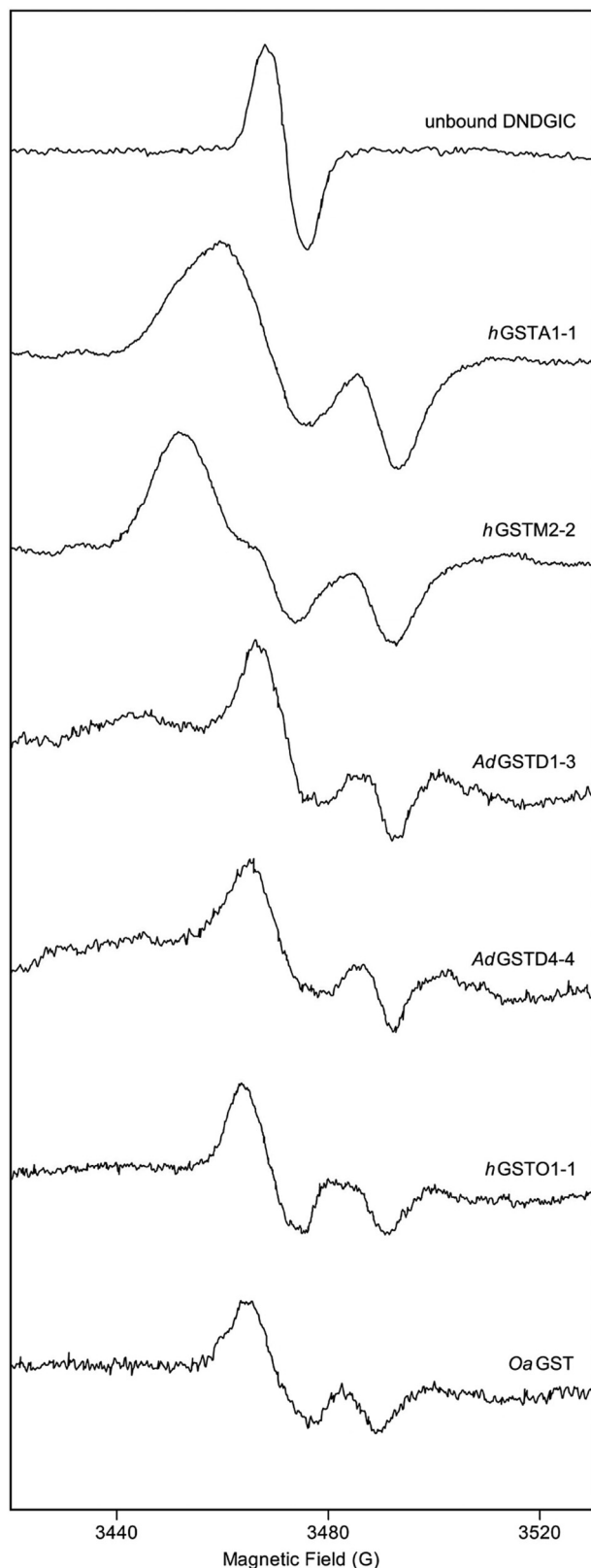
FIGURE 3. EPR experiments. EPR spectra at 22–25 °C of DNGIC bound to representative GSTs belonging to Tyr-GSTs (*h*GSTA1-1 and *h*GSTM2-2), Ser-GSTs (GSTD1-3, GSTD4-4), and Cys-GSTs (*h*GSTO1-1 and *Oa*GST). Experiments were performed as described under "Experimental Procedures."

strong affinity found in the Tyr-GSTs is, in part, due to a much more pronounced deprotonation of their crucial residue (the average pK_a for Tyr = 8.9). The poor affinity found in the Cys-GSTs is caused by different factors. The Cys residue should be an ideal coordination ligand for the iron and the mean pK_a value of its sulfhydryl group in all Cys-GSTs studied is only 7.8. However, the docked structure of DNGIC in these GSTs shows a GSH incorrectly bound to the G-site with a geometry significantly different from the one observed in the crystal structures of the Cys-GST·GSH complexes, as indicated by the relatively high root mean square deviation of GSH from its crystallographic position (Table 2). It appears that the formation of the fourth coordination link of the iron with the Cys residue does not allow GSH to bind properly, loosing most of its favorable interactions with the G-site. By contrast, in the final docked conformation of most Tyr-GSTs the GSH was positioned essentially in the same way as observed in the corresponding crystal structures of GST·GSH complexes.

Isoelectric Points and K_D for DNDGIC Are Correlated—A surprising finding about the Tyr-GST isoenzymes is the correlation between the net charge of these proteins and their affinities for DNDGIC ($r^2 = 0.92$; $p < 0.001$) (Fig. 5A). In particular, the isoenzymes with the greatest affinity among all Tyr-GSTs considered are also those showing the highest isoelectric points (Table 2). For example, the human GSTA1-1 and GSTA3-3 (pI = 9.4 and 9.7) display K_D values less than 10^{-10} M, whereas the *h*GSTP1-1 (pI = 6.0) has K_D value about 25-fold higher. This finding is likely related to the influence of positive charges on the deprotonation of the crucial Tyr in the G-site, as indicated by the correlation between pI and its pK_a (Fig. 5B). On the contrary, poor or even no correlation between pI and K_D occurs for the Ser-GSTs ($r^2 = 0.74$; $p = 0.03$) and Cys-GSTs ($r^2 = 0.02$; $p = 0.78$) (not shown). In addition, we noted that a strong cationic character is almost exclusively observed in the more recently evolved GSTs, *i.e.* in the Tyr-GSTs and, in particular, in the Alpha class GSTs reaching a pI of 9.5–9.7. Among all Ser-GSTs only two isoenzymes show pI values higher than 8.0 and only one Cys-GST displays pI > 7.5. As discussed below, the correlation between net charge and affinity for DNDGIC as well as the particular distribution of the positive residues in the Tyr-GSTs (Fig. 5C) may have interesting physiological implications.

DISCUSSION

The present study, which includes experimental data for 23 purified GSTs and analysis of 42 crystal structures of different isoenzymes belonging to the Tyr/Ser/Cys GST subfamilies, provides coherent evidence that the Cys/Ser/Tyr replacements during evolution have not been selected to improve binding or activation of GSH, but to optimize the binding of DNDGIC and thus increase the protection of the cell against NO toxicity. Experimental data indicate that only the Tyr-GSTs members reach the astonishing K_D range of 10^{-9}–10^{-11} M and, from theoretical calculation, even 10^{-14} M for the mouse and chicken GSTA1-1 (Table 2). Conversely, Ser-GSTs display affinities 10^2–10^4 times lower and even less affinity has been observed for the Cys-GST members. The reasons for this poor affinity are the very low acidity of the hydroxyl group of the Ser residue and the unfavorable stereochemical factors for the Cys-GSTs, as
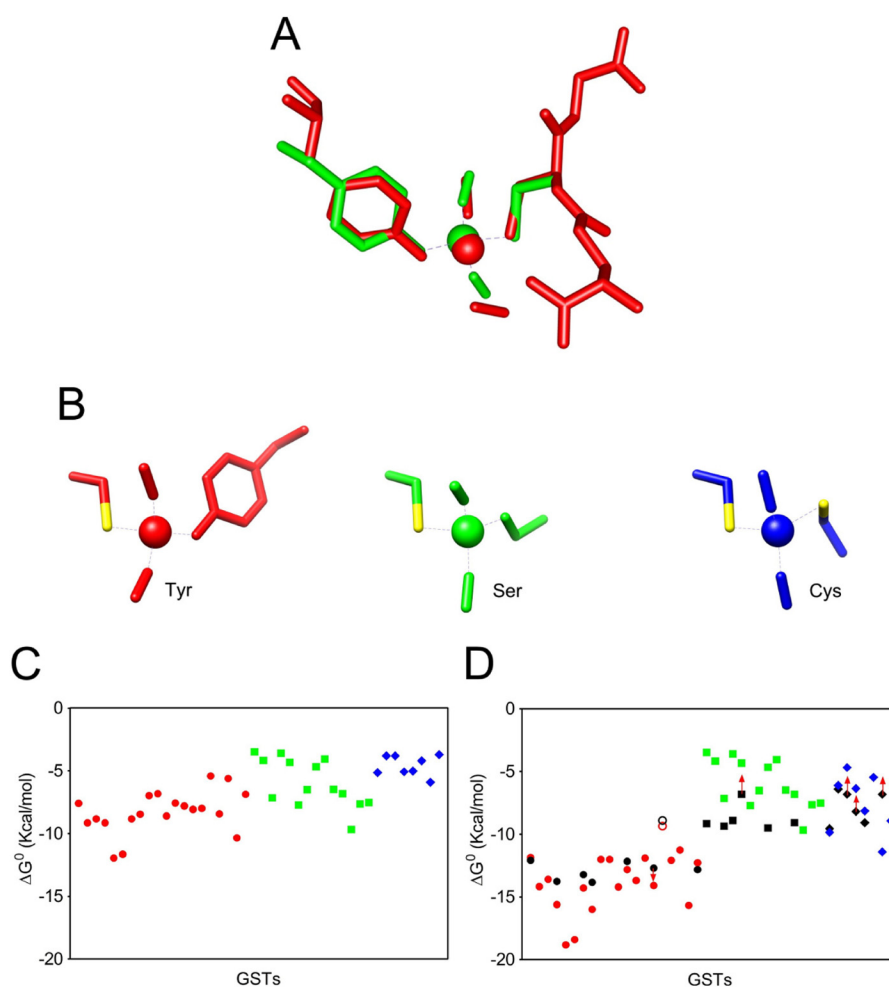
FIGURE 4. **Experimental and theoretical studies of DNGIC binding to GSTs.** *A,* DNGIC·GST complex structure as obtained from DFT calculations (*green*) superimposed on the crystallographic model (*red*) (PDB code 1ZGN). *B,* structures of DNGIC with Tyr (*red*), Ser (*green*), and Cys (*blue*) as fourth ligands, obtained from DFT calculations. *C,* free energy of the GST/DNGIC interaction obtained from docking calculations. Tyr-GSTs (*red circle*), Ser-GSTs (*green square*), and Cys-GSTs (*blue triangle*). *D,* free energies of GST/DNGIC interaction as in *C* were corrected for the energy of the coordination bond involving the Tyr residue (-4.1 kcal/mol for a Tyr with a $pK_a = 9.8$ as in GSTP1-1) and the Cys residue (-3.3 kcal/mol for a Cys with $pK_a = 7.3$ as in GSTB1-1). Coordination energy due to Tyr or Cys residues with different pK_a have been calculated as described under "Experimental Procedures." Symbols are as described in *C. Black symbols* are experimental K_D values, whereas the corresponding theoretical K_D values are reported with the same vertical alignment. Starting from left, data refer to GSTs in the same sequence of that reported in Table 1 (excluding the five mutants), *red open circle* and *black open circle* are the theoretical and experimental energy values for the atypical *Pf*GST. *Red arrow* indicates that the true ΔG^0 value could be even more (*red arrow ↓*) or less (*red arrow ↑*) negative (higher or lower affinity, respectively).

confirmed by site-directed mutagenesis data and docking studies. Furthermore, an additional property of the Cys-GSTs makes this subfamily unsuitable to bind DNDGIC efficiently. *In vivo*, most of the Cys-GSTs exist mainly in a mixed disulfide form involving GSH and the essential Cys. It has been found that this oxidized disulfide is strongly favored even when the GSH/GSSG ratio is higher than 100, *i.e.* when only traces of GSSG are present in the cell (53). In this form the G-site is not able to accommodate DNGIC. The NO sensitivity of bacteria that express only Cys-GSTs could be related to the low or null affinity of their Cys-GSTs for DNDGIC.

In a physiological scenario, what is the utility or the necessity to reach such extremely high affinities like those observed in the Tyr-GST subfamily (10^{-9}–10^{-11} M)? A plausible explanation is given in the "traffic light" graph in Fig. 5D. This panel shows the predicted inhibition of glutathione reductase, an enzyme crucial for cell redox equilibrium, which is strongly inactivated by the free DNDGIC with a $K_i = 3$ μM (10). In the case of DNDGIC

production that is stoichiometric with GST, only the Tyr-GSTs confer efficient enzyme protection. A similar protection scenario occurs in case of substoichiometric amounts of DNDGIC. Obviously, a dramatic inactivation occurs even in the presence of Tyr-GSTs when DNDGIC is in stoichiometric excess, as demonstrated previously (11). As emphasized by Karplus and co-workers, the cell needs to be efficiently protected from DNDGIC (9) and it is now evident that only in the presence of very efficient DNDGIC traps like Tyr-GSTs, the level of this iron complex stays far below its lethal concentration (Fig. 5D).

It is likely that the Tyr adaptation occurred in a common ancestor of the current metazoan species over 500 million years ago (54) and has been maintained by selection during the subsequent speciation. Gene duplication and mutation followed by selection by other factors has likely generated the multiplicity of Tyr-containing enzymes with different substrate specificities that we find today. However, because DNDGIC remains an intracellular toxin, the selection pressure to retain GSTs with

TABLE 2
Thermodynamic and geometric parameters from docking studies of DNDGIC and pK_a of the essential residue

PDB ID	GSTs	ΔG^0 for DNDGIC-GSTs interaction	Theoretical K_D DNDGIC	Root mean square deviation[a]	pK_a of the essential residue	pI
		kcal/mol	*M*	*Å*		
Tyrosine subfamily						
6GSS	*h*GSTP1-1	−12.04	1.5×10^{-9}	0.463	9.84	6.0
1GLP	*m*GSTYfYf	−14.17	4.1×10^{-11}	0.629	9.15	8.9
1TU8	*O. volvulus* GST2	−13.58	1.1×10^{-10}	0.614	9.38	7.7
1K3L	*h*GSTA1-1	−15.61	3.6×10^{-12}	1.457	8.10	9.4
1F3A	*m*GSTA1-1	−18.82	1.6×10^{-14}	0.353	7.81	9.6
1VF2	*c*GSTA1-1	−18.39	3.3×10^{-14}	0.806	7.90	9.4
2WJU	*h*GSTA2-2	−14.28	3.4×10^{-11}	0.474	8.85	8.7
1TDI	*h*GSTA3-3	−15.99	1.9×10^{-12}	0.751	7.31	9.7
1GUL	*h*GSTA4-4	−12.00	1.6×10^{-9}	0.874	9.17	7.3
1B48	*m*GSTA4-4	−12.00	1.6×10^{-9}	1.412	9.04	8.2
1GSU	*c*GSTM1-1	−14.20	3.9×10^{-11}	0.320	8.73	7.6
2AB6	*h*GSTM2-2	−12.82	4.0×10^{-10}	0.347	8.99	7.1
6GST	*r*GSTM3-3	−13.70	9.0×10^{-11}	1.263	8.52	8.6
1M9A	*S. japonicum* GST	−11.90	1.9×10^{-9}	0.618	10.05	6.3
1OE7	*S. haematobium* GST	−14.08	4.8×10^{-11}	0.603	8.38	8.0
1Q4J	*P. falciparum* GST	−9.35	1.4×10^{-7}	0.503	9.93	6.7
1U3I	*S. mansoni* GST	−12.08	1.4×10^{-9}	0.624	10.18	7.3
2ON5	*N. americanus* GST	−11.27	5.5×10^{-9}	2.016	8.68	8.6
2WB9	*F. hepatica* GST	−15.66	3.3×10^{-12}	0.488	8.94	9.4
1GSQ	Squid GSTS	−12.28	9.9×10^{-10}	0.758	8.88	8.6
Serine subfamily						
1AXD	Phi 1 GST Mais	−3.48	2.8×10^{-3}	4.638	11.46	5.5
	L. cuprina GST	−4.17	8.8×10^{-4}	0.919	13.16	
1JLV	*Ad*GSTD3-3	−7.15	5.7×10^{-6}	0.462	12.43	6.8
3LJR	*h*GSTT2-2	−3.60	2.3×10^{-3}	3.319	11.35	6.6
1FW1	*h*GSTZ1-1	−4.33	6.7×10^{-4}	11.162	9.32	9.1
1GWC	*Ta*GSTU4-4	−7.72	2.2×10^{-6}	0.788	11.69	6.0
1PN9	*Ag*GSTD1-6	−6.51	1.7×10^{-5}	0.453	13.11	6.5
1R5A	*Ad*GSTD5-5	−4.67	3.8×10^{-4}	0.770	13.65	6.1
2C3Q	*h*GSTT1-1	−4.04	1.1×10^{-3}	8.110	11.94	8.6
2IMI	*Ag*GSTE2	−6.47	1.8×10^{-5}	0.846	14.34	5.7
3F63	*Ad*GSTD4-4	−6.82	1.0×10^{-5}	0.352	12.20	5.2
3M0F	*P. fluorescens* GST	−9.68	8.0×10^{-8}	0.858	11.68	6.1
3UBL	*L. interrogans* GST	−7.64	2.5×10^{-6}	1.672	11.64	7.3
3TOU	*R. solanacearum* GST	−7.51	3.1×10^{-6}	1.362	10.27	6.0
Cysteine subfamily						
1EEM	*h*GSTO1-1	−9.69	7.9×10^{-8}	3.165	6.69	8.0
2PMT	*P. mirabilis* GSTB1-1	−6.31	2.4×10^{-5}	3.167	8.19	7.3
1F2E	*S. paucimobilis* GST	−4.68	3.7×10^{-4}	10.006	9.42	5.3
2DSA	*B. xenovorans* GST	−6.35	2.2×10^{-5}	1.290	9.06	6.1
2NTO	*O. anthropi* GST	−8.34	7.7×10^{-7}	1.210	7.63	6.8
2X64	*X. fastidiosa* GST	−5.47	9.8×10^{-5}	3.886	9.06	7.5
3N5O	*C. immitis* GST	−11.40	4.4×10^{-9}	7.019	5.98	7.2
3UAR	*M. capsulatus* GST	−8.94	2.8×10^{-7}	8.000	6.23	4.9

[a] Root mean square deviation between crystallographic and "docked" GSH structures obtained from DNGIC docking.

Tyr residues also remains. Indirect but convincing evidence for the link between GST evolution and NO is given by the anomalous poor affinity of *P. falciparum* GST for DNDGIC. This Tyr-GST shows 100 times less affinity than all other Tyr-GSTs and an appealing explanation for this peculiarity is that the parasite, living in an environment containing a very high hemoglobin concentration, is strongly protected from NO, given that hemoglobin is an efficient scavenger of this compound (55). Thus, this enzyme did not need to refine its affinity for DNDGIC during evolution or, alternatively, in an early stage of evolution this parasite developed an efficient NO defense (with a Tyr-GST), which became redundant when it installed itself inside the erythrocyte. Inspection of its G-site reveals an unfavorable charge distribution near the binding site (not involving the essential Tyr, which display a K_a very similar to that of GSTP1-1). We conclude that the presence of Tyr in the active site of GSTs is a necessary but not sufficient condition to reach affinities in the low nanomolar range. Obviously, our data do not provide any definitive proof for the link between GST evolution and NO or DNDGIC protection; we cannot exclude that

the observed parallelism (*i.e.* only the more recently evolved GSTs may efficiently inactivate dinitrosyl·iron complexes) could be merely coincidental.

A second important finding from this study is that the most avid GSTs acting as scavengers for DNDGIC are also those with the most prominent cationic character, *i.e.* those having the highest pI values (Fig. 5*A*). The positive electrostatic potential in the Tyr-GSTs may have a double function. First, the presence of discrete positively charges localized near the G-site lowers the pK_a of the essential Tyr residue (from 10.2 to 7.3 with an average value of 8.9) favoring its coordination with iron. The second function is related to the involvement of the cationic GSTs in a peculiar intracellular structure. It has been demonstrated recently that, in mammalian liver cells, highly cationic Tyr-GSTs (GSTA1-1, GSTA2-2, and GSTA3-3) are present in the cytosol, but are also over-represented in a perinuclear crowd of cationic enzymes termed the "nuclear shield." This structure, about 300 nm thick around the nuclear membrane, is promoted by electrostatic interactions, and it is possibly selected for DNA protection (56). In fact, the local concentra-
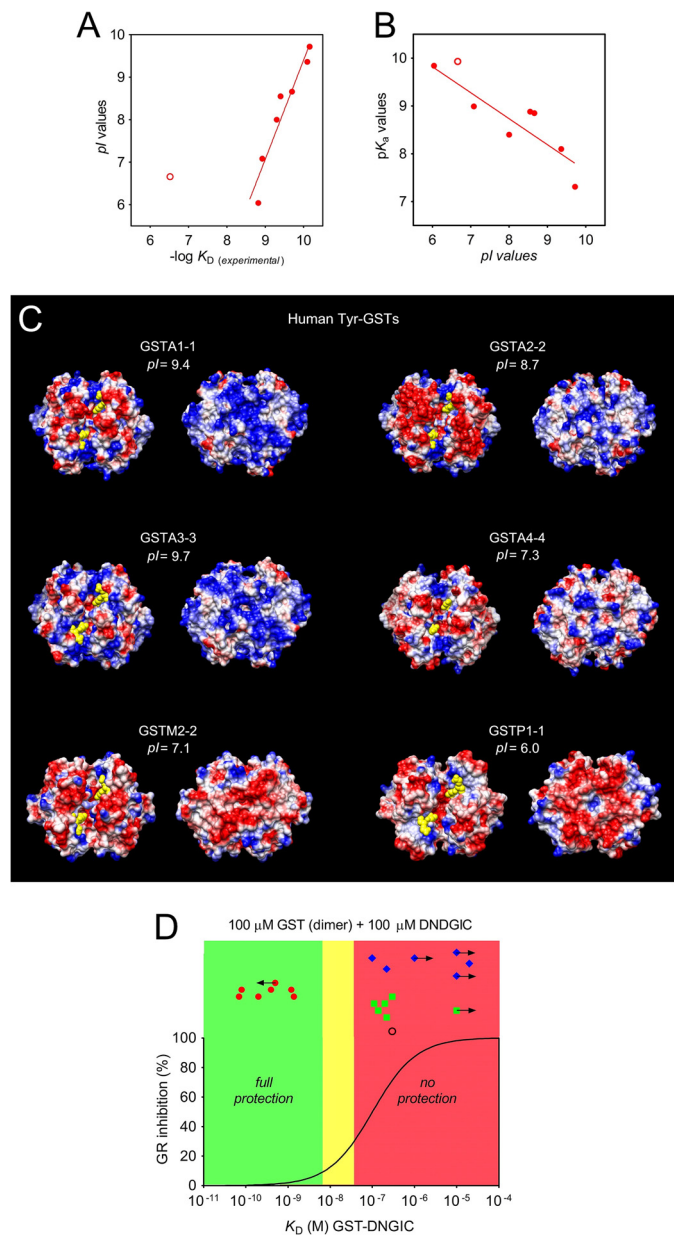
FIGURE 5. **The role of protein charge.** *A,* dependence of the affinity of GSTs for DNDGIC as a function of pI values for Tyr-GSTs (*red circle*), *Pf*GST (*red open circle*) ($r^2 = 0.92$; $p < 0.001$) excluding the anomalous *Pf*GST. *B,* correlation between pI and pK_a values of the catalytic residues of Tyr-GSTs. Linear regression shows positive correlation ($r^2 = 0.78$, $p = 0.009$). Tyr-GSTs, *red circle*; *Pf*GST, *red open circle*. Ser- and Cys-GSTs did not show correlations. *C,* coulombic potential on the dimer surface of selected Tyr-GSTs facing the two G-sites (models on *left*) and opposite to the G-sites (models on *right*). Glutathione is represented as *yellow spheres*. The protein surface is colored based on the electrostatic potential values, as *red* (negative values), *blue* (positive values), or *white* (near zero values) in the range −5 to +5 kcal/(mol·e). *D,* "traffic light" graph. Predictive dependence of GR inhibition (%) in the presence of a stoichiometric amount of GSTs (site at high affinity) and DNDGIC, as a function of experimental K_D for DNDGIC. On the basis of the K_D, the unbound DNDGIC and then the percentage of GR inhibition ($K_i = 3$ μM) (*continuous line*) (9, 10) were calculated. Good protection is assumed for inhibition less than 10%. Low or no protection is assumed for inhibition >30%. Tyr-GST (*red circle*), *Pf*GST (*black open circle*), Ser-GST (*green square*), and Cys-GST (*blue triangle*). *Arrow* indicates that K_D measured by EPR experiments could be even lower (←) or higher (→). See also Table 1.

tion of GSTs in the shield is 7–8 times higher than that found in the cytosol (56). GSTA4-4 and Mu class GSTs, which are abundantly expressed in hepatocytes but with less cationic character

and also less affinity for DNDGIC, are absent in this structure (56). Conversely, other important protection enzymes with strong cationic character form part of this perinuclear structure that probably uses the nesprins (large anionic proteins localized on the outer nuclear membrane) as an electrostatic counterpart (56). The particular distribution of positively charged residues observed in the dimer surface of Alpha GSTs (Fig. 5*C*), *i.e.* in the side apposite to the G-sites, appears to be convenient for the involvement of these proteins in the *nuclear shield*: it makes an efficient electrostatic protein-protein interaction somehow without obscuring the active site used for DNDGIC binding or catalysis.

Thus, we speculate that GSTs evolved to protect not only key cytosolic enzymes like glutathione reductase against NO insults, but possibly even DNA or intra-nuclear related enzymes. It has been reported that dinitrosyl·iron complexes induce the SOS DNA repair response in *Escherichia coli* and that DNDGIC is the most potent SOS inducer (57). Recently, it has been found that in *E. coli* the DinG (4Fe-4S) cluster can efficiently bind the dinitrosyl·iron complex with the concomitant inactivation of helicase activity *in vitro* and *in vivo* (58). Because genetic defects in the human XPD gene (*ERCC2*) have been associated with the increase of cancer incidence and aging phenotypes (59–62), it is plausible that chronic NO or DNDGIC exposure may inactivate the iron-sulfur cluster-containing DNA repair enzymes such as DinG/XPD and contribute to the initiation of the carcinogenic process and genomic instability (63, 64). Therefore, the accumulation of the most potent DNDGIC scavengers (GSTA1-1, GSTA2-2, and GSTA3-3) around the nucleus could be of paramount importance. Thus it may not be coincidental that the cationic GSTs are exclusively found in more recently evolved eukaryotes. In conclusion, we propose a fascinating and novel hypothesis about GST evolution and protection against NO that opens up new perspectives in cell physiology.

REFERENCES

1. Armstrong, R. N. (1997) Structure, catalytic mechanism, and evolution of the glutathione transferases. *Chem. Res. Toxicol.* **10,** 2–18
2. Hayes, J. D., Flanagan, J. U., and Jowsey, I. R. (2005) Glutathione transferases. *Annu. Rev. Pharmacol. Toxicol.* **45,** 51–88
3. Mannervik, B., Board, P. G., Hayes, J. D., Listowsky, I., and Pearson, W. R. (2005) Nomenclature for mammalian soluble glutathione transferases. *Methods Enzymol.* **401,** 1–8
4. Nebert, D. W., and Vasiliou, V. (2004) Analysis of the glutathione *S*-transferase (GST) gene family. *Hum. Genomics* **1,** 460–464
5. Atkinson, H. J., and Babbitt, P. C. (2009) Glutathione Transferases are structural and functional outliers in the thioredoxin fold. *Biochemistry* **48,** 11108–11116
6. Sheehan, D., Meade, G., Foley, V. M., and Dowd, C. A. (2001) Structure, function and evolution of glutathione transferases. Implications for classification of non-mammalian members of an ancient enzyme superfamily. *Biochem. J.* **360,** 1–16
7. Hill, B. G., Dranka, B. P., Bailey, S. M., Lancaster, J. R., Jr., and Darley-Usmar, V. M. (2010) What part of NO don't you understand? Some answers to the cardinal questions in nitric oxide biology. *J. Biol. Chem.* **285,** 19699–19704

8. Ueno, T., and Yoshimura, T. (2000) The physiological activity and in vivo distribution of dinitrosyl dithiolato iron complex. *Jpn. J. Pharmacol.* **82,** 95–101

9. Becker, K., Savvides, S. N., Keese, M., Schirmer, R. H., and Karplus, P. A. (1998) Enzyme inactivation through sulphydryl oxidation by physiologic NO-carriers. *Nat. Struct. Biol.* **5,** 267–271

10. Keese, M. A., Böse, M., Mülsch, A., Schirmer, R. H., and Becker, K. (1997) Dinitrosyl-dithiol-iron complexes, nitric oxide (NO) carriers *in vivo*, as potent inhibitors of human glutathione reductase and glutathione *S*-transferase. *Biochem. Pharmacol.* **54,** 1307–1313

11. Pedersen, J. Z., De Maria, F., Turella, P., Federici, G., Mattei, M., Fabrini, R., Dawood, K. F., Massimi, M., Caccuri, A. M., and Ricci, G. (2007) Glutathione transferases sequester toxic dinitrosyl-iron complexes in cells. A protection mechanism against excess nitric oxide. *J. Biol. Chem.* **282,** 6364–6371

12. De Maria, F., Pedersen, J. Z., Caccuri, A. M., Antonini, G., Turella, P., Stella, L., Lo Bello, M., Federici, G., and Ricci, G. (2003) The specific interaction of dinitrosyl-diglutathionyl-iron complex, a natural NO carrier, with the glutathione transferase superfamily. Suggestion for an evolutionary pressure in the direction of the storage of nitric oxide. *J. Biol. Chem.* **278,** 42283–42293

13. Turella, P., Pedersen, J. Z., Caccuri, A. M., De Maria, F., Mastroberardino, P., Lo Bello, M., Federici, G., and Ricci, G. (2003) Glutathione transferase superfamily behaves like storage proteins for dinitrosyl-diglutathionyl-iron complex in heterogeneous systems. *J. Biol. Chem.* **278,** 42294–42299

14. Lo Bello, M., Nuccetelli, M., Caccuri, A. M., Stella, L., Parker, M. W., Rossjohn, J., McKinstry, W. J., Mozzi, A. F., Federici, G., Polizio, F., Pedersen, J. Z., and Ricci, G. (2001) Human glutathione transferase P1-1 and nitric oxide carriers. A new role for an old enzyme. *J. Biol. Chem.* **276,** 42138–42145

15. Tetlow, N., and Board, P. G. (2004) Functional polymorphism of human glutathione transferase A2. *Pharmacogenetics* **14,** 111–116

16. Tetlow, N., Coggan, M., Casarotto, M. G., and Board, P. G. (2004) Functional polymorphism of human glutathione transferase A3. Effects on xenobiotic metabolism and steroid biosynthesis. *Pharmacogenetics* **14,** 657–663

17. Höppner, J., Perbandt, M., Betzel, Ch., Walter, R. D., and Liebau, E. (2004) Crystallization of the major cytosolic glutathione *S*-transferase from *Onchocerca volvulus. Acta Crystallogr. D* **60,** 1496–1497

18. Johnson, K. A., Angelucci, F., Bellelli, A., Hervé, M., Fontaine, J., Tsernoglou, D., Capron, A., Trottein, F., and Brunori, M. (2003) Crystal structure of the 28-kDa glutathione *S*-transferase from *Schistosoma haematobium. Biochemistry* **42,** 10084–10094

19. Harwaldt, P., Rahlfs, S., and Becker, K. (2002) Glutathione *S*-transferase of the malarial parasite *Plasmodium falciparum.* Characterization of a potential drug target. *Biol. Chem.* **383,** 821–830

20. Tomarev, S. I., Zinovieva, R. D., Guo, K., and Piatigorsky, J. (1993) Squid glutathione *S*-transferase. *J. Biol. Chem.* **268,** 4534–4542

21. Caccuri, A. M., Antonini, G., Board, P. G., Flanagan, J., Parker, M. W., Paolesse, R., Turella, P., Federici, G., Lo Bello, M., and Ricci, G. (2001) Human glutathione transferase T2-2 discloses some evolutionary strategies for optimization of substrate binding to the active site of glutathione transferases. *J. Biol. Chem.* **276,** 5427–5431

22. Mozer, T. J., Tiemeier, D. C., and Jaworski, E. G. (1983) Purification and characterization of corn glutathione *S*-transferase. *Biochemistry* **22,** 1068–1072

23. Tzeng, H. F., Blackburn, A. C., Board, P. G., and Anders, M. W. (2000) Polymorphism- and species-dependent inactivation of glutathione transferase ζ by dichloroacetate. *Chem. Res. Toxicol.* **13,** 231–236

24. Oakley, A. J., Harnnoi, T., Udomsinprasert, R., Jirajaroenrat, K., Ketterman, A. J., and Wilce, M. C. (2001) The crystal structures of glutathione *S*-transferases isozymes 1–3 and 1–4 from *Anopheles dirus* species B. *Protein Sci.* **10,** 2176–2185

25. Wongsantichon, J., Robinson, R. C., and Ketterman, A. J. (2010) Structural contributions of delta class glutathione transferase active-site residues to catalysis. *Biochem. J.* **428,** 25–32

26. Udomsinprasert, R., Pongjaroenkit, S., Wongsantichon, J., Oakley, A. J., Prapanthadara, L. A., Wilce, M. C., and Ketterman, A. J. (2005) Identifica-tion, characterization and structure of a new Delta class glutathione transferase isoenzyme. *Biochem. J.* **388,** 763–771

27. Board, P. G., Coggan, M., Chelvanayagam, G., Easteal, S., Jermiin, L. S., Schulte, G. K., Danley, D. E., Hoth, L. R., Griffor, M. C., Kamath, A. V., Rosner, M H., Chrunyk, B. A., Perregaux, D. E., Gabel, C. A., Geoghegan, K. F., and Pandit, J. (2000) Identification, characterization, and crystal structure of the Omega class glutathione transferases. *J. Biol. Chem.* **275,** 24798–24806

28. Fortin, P. D., Horsman, G. P., Yang, H. M., and Eltis, L. D. (2006) A glutathione *S*-transferase catalyzes the dehalogenation of inhibitory metabolites of polychlorinated biphenyls. *J. Bacteriol.* **188,** 4424–4430

29. Favaloro, B., Tamburro, A., Angelucci, S., Luca, A. D., Melino, S., di Ilio, C., and Rotilio, D. (1998) Molecular cloning, expression and site-directed mutagenesis of glutathione *S*-transferase from *Ochrobactrum anthropi. Biochem. J.* **335,** 573–579

30. Edwards, T. E., Bryan, C. M., Leibly, D. J., Dieterich, S. H., Abendroth, J., Sankaran, B., Sivam, D., Staker, B. L., Van Voorhis, W. C., Myler, P. J., and Stewart, L. J. (2011) Structures of a putative ζ-class glutathione *S*-transferase from the pathogenic fungus *Coccidioides immitis. Acta Crystallogr. Sect. F Struct. Biol. Cryst. Commun.* **67,** 1038–1043

31. Cesareo, E., Parker, L. J., Pedersen, J. Z., Nuccetelli, M., Mazzetti, A. P., Pastore, A., Federici, G., Caccuri, A. M., Ricci, G., Adams, J. J., Parker, M. W., and Lo Bello, M. (2005) Nitrosylation of human glutathione transferase P1-1 with dinitrosyl diglutathionyl iron complex *in vitro* and *in vivo. J. Biol. Chem.* **280,** 42172–42180

32. Tan, K. L., Chelvanayagam, G., Parker, M. W., and Board, P. G. (1996) Mutagenesis of the active site of the human Theta-class glutathione transferase GSTT2-2. Catalysis with different substrates involves different residues. *Biochem. J.* **319,** 315–321

33. Caccuri, A. M., Antonini, G., Allocati, N., Di Ilio, C., De Maria, F., Innocenti, F., Parker, M. W., Masulli, M., Lo Bello, M., Turella, P., Federici, G., and Ricci, G. (2002) GSTB1-1 from *Proteus mirabilis.* A snapshot of an enzyme in the evolutionary pathway from a redox enzyme to a conjugating enzyme. *J. Biol. Chem.* **277,** 18777–18784

34. Allocati, N., Federici, L., Masulli, M., Favaloro, B., and Di Ilio, C. (2008) Cysteine 10 is critical for the activity of *Ochrobactrum anthropi* glutathione transferase and its mutation to alanine causes the preferential binding of glutathione to the H-site. *Proteins* **71,** 16–23

35. Hohenberg, P., and Kohn, W. (1964) Inhomogeneous electron gas. *Phys. Rev. B* **136,** 864–871

36. Kohn, W., and Sham, L. J. (1965) Self-consistent equations including exchange and correlations effects. *Phys. Rev.* **140,** 1133–1138

37. Noodleman, L., Case, D. A., and Aizman, A. (1988) Broken symmetry analysis of spin coupling in iron-sulfur clusters. *J. Am. Chem. Soc.* **110,** 1001–1005

38. Neese, F. (2012) The ORCA program system. *WIREs Comput. Mol. Sci.* **2,** 73–78

39. Neese, F. (2000) Approximate Second Order Convergence for Spin Unrestricted Wavefunctions. *Chem. Phys. Lett.* **325,** 93–98

40. Ye, S., and Neese, F. (2010) The unusual electronic structure of dinitrosyl iron complexes. *J. Am. Chem. Soc.* **132,** 3646–3647

41. Morris, G. M., Goodsell, D. S., Halliday, R. S., Huey, R., Hart, W. E., Belew, R. K., and Olson, A. J. (1998) Automated docking using a Lamarckian Genetic Algorithm and empirical binding free energy function. *J. Comput. Chem.* **19,** 1639–1662

42. Morris, G. M., Huey, R., Lindstrom, W., Sanner, M. F., Belew, R. K., Goodsell, D. S., and Olson, A. J. (2009) AutoDock4 and AutoDockTools4. Automated docking with selective receptor flexibility. *J. Comput. Chem.* **30,** 2785–2791

43. Gasteiger, J., and Marsili, M. (1980) Iterative partial equalization of orbital electronegativity. A rapid access to atomic charges. *Tetrahedron* **36,** 3219–3228

44. Singh, U. C., and Kollman, P. A. (1984) An approach to computing electrostatic charge for molecules. *J. Comp. Chem.* **5,** 129–145

45. Baker, N. A., Sept, D., Joseph, S., Holst, M. J., and McCammon, J. A. (2001) Electrostatics of nanosystems. Application to microtubules and the ribosome. *Proc. Natl. Acad. Sci. U.S.A.* **98,** 10037–10041

46. Dolinsky, T. J., Nielsen, J. E., McCammon, J. A., and Baker, N. A. (2004)

PDB2PQR. An automated pipeline for the setup, execution, and analysis of Poisson-Boltzmann electrostatics calculations. *Nucleic Acids Res.* **32,** W665–667

47. Sitkoff, D., Sharp, K. A., and Honig, B. (1994) Accurate calculation of hydration free energies using macroscopic solvent models. *J. Phys. Chem.* **98,** 1978–1988

48. Pettersen, E. F., Goddard, T. D., Huang, C. C., Couch, G. S., Greenblatt, D. M., Meng, E. C., and Ferrin, T. E. (2004) UCSF Chimera. A visualization system for exploratory research and analysis. *J. Comput. Chem.* **13,** 1605–1612

49. Fahey, R. C., and Sundquist, A. R. (1991) Evolution of glutathione metabolism. *Adv. Enzymol. Relat. Areas Mol. Biol.* **64,** 1–53

50. Caccuri, A. M., Lo Bello, M., Nuccetelli, M., Nicotra, M., Rossi, P., Antonini, G., Federici, G., and Ricci, G. (1998) Proton release upon glutathione binding to glutathione transferase P1-1. Kinetic analysis of a multistep glutathione binding process. *Biochemistry* **37,** 3028–3034

51. Caccuri, A. M., Antonini, G., Board, P. G., Parker, M. W., Nicotra, M., Lo Bello, M., Federici, G., and Ricci, G. (1999) Proton release on binding of glutathione to Alpha, Mu and Delta class glutathione transferases. *Biochem. J.* **344,** 419–425

52. Flatgaard, J. E., Bauer, K. E., and Kauvar, L. M. (1993) Isozyme specificity of novel glutathione-*S*-transferase inhibitors. *Cancer Chemother. Pharmacol.* **33,** 63–70

53. Caccuri, A. M., Antonini, G., Allocati, N., Di Ilio, C., Innocenti, F., De Maria, F., Parker, M. W., Masulli, M., Polizio, F., Federici, G., and Ricci, G. (2002) Properties and utility of the peculiar mixed disulfide in the bacterial glutathione transferase B1-1. *Biochemistry* **41,** 4686–4693

54. Pearson, W. R. (2005) Phylogenies of glutathione transferase families. *Methods Enzymol.* **401,** 186–204

55. Azarov, I., Huang, K. T., Basu, S., Gladwin, M. T., Hogg, N., and Kim-Shapiro, D. B. (2005) Nitric oxide scavenging by red blood cells as a function of hematocrit and oxygenation. *J. Biol. Chem.* **280,** 39024–39032

56. Fabrini, R., Bocedi, A., Pallottini, V., Canuti, L., De Canio, M., Urbani, A., Marzano, V., Cornetta, T., Stano, P., Giovanetti, A., Stella, L., Canini, A., Federici, G., and Ricci, G. (2010) Nuclear shield. A multi-enzyme task-force for nucleus protection. *PLoS One* **5,** e14125

57. Lobysheva, I. I., Stupakova, M. V., Mikoyan, V. D., Vasilieva, S. V., and Vanin, A. F. (1999) Induction of the SOS DNA repair response in *Escherichia coli* by nitric oxide donating agents. Dinitrosyl iron complexes with thiol-containing ligands and S-nitrosothiols. *FEBS Lett.* **454,** 177–180

58. Ren, B., Duan, X., and Ding, H. (2009) Redox control of the DNA damage-inducible protein DinG helicase activity via its iron-sulfur cluster. *J. Biol. Chem.* **284,** 4829–4835

59. Lehmann, A. R. (2001) The *Xeroderma pigmentosum* group D (XPD) gene. One gene, two functions, three diseases. *Genes Dev.* **15,** 15–23

60. Liu, H., Rudolf, J., Johnson, K. A., McMahon, S. A., Oke, M., Carter, L., McRobbie, A. M., Brown, S.E., Naismith, J. H., and White, M. F. (2008) Structure of the DNA repair helicase XPD. *Cell* **133,** 801–812

61. Fan, L., Fuss, J. O., Cheng, Q. J., Arvai, A. S., Hammel, M., Roberts, V. A., Cooper, P. K., and Tainer, J. A. (2008) XPD helicase structures and activities. Insights into the cancer and aging phenotypes from XPD mutations. *Cell* **133,** 789–800

62. Rudolf, J., Makrantoni, V., Ingledew, W. J., Stark, M. J., and White, M. F. (2006) The DNA repair helicases XPD and FancJ have essential iron-sulfur domains. *Mol. Cell* **23,** 801–808

63. Gal, A., and Wogan, G. N. (1996) Mutagenesis associated with nitric oxide production intransgenic SJL mice. *Proc. Natl. Acad. Sci. U.S.A.* **93,** 15102–15107

64. Li, C. Q., Trudel, L. J., and Wogan, G. N. (2002) Nitric oxide-induced genotoxicity, mitochondrial damage, and apoptosis in human lymphoblastoid cells expressing wild-type and mutant p53. *Proc. Natl. Acad. Sci. U.S.A.* **99,** 10364–10369